Investigating the Effects of Land Use Change on Subsurface, Surface and Atmospheric Branches of the Hydrologic Cycle in central Argentina

Sujan Pal[1], Francina Dominguez[2], Pablo Bollatti[3], Yi Yang[4], Javier Alvarez[5], and Carlos Marcelo Garcia[6]

[1]University of Illinois at Urbana Champaign
[2]University of Illinois at Urbana-Champaign-Department of Atmospheric Sciences
[3]Instituto National de Technologi a Agropecuaria
[4]University of Illinois at Urbana-Champaign
[5]Institute for Advanced Studies for Engineering and Technology (IDIT CONICET-UNC) and Exact, Physical and Natural Sciences College, National University of Córdoba, (FCEFyN - UNC)
[6]Universidad Nacional de Córdoba

November 22, 2022

Abstract

Since the 1970s, agricultural production in central Argentina has shifted away from perennial crops and grasses towards annual crops, largely soy. In this work we use observations and modeling to understand how this shift in land cover has affected the sub-surface, surface and atmospheric fluxes of moisture and energy in a flat agricultural area. We analyze the flux tower data from a paired site at Marcos Juarez in central Argentina during the period of the RELAMPAGO field campaign (2018-2019). When compared to perennial alfalfa, the observations over soy show lower evapotranspiration and specific humidity, higher sensible heat, higher outgoing shortwave radiation and soil temperature. Furthermore, water table depth is shallower below the soy than the alfalfa sites. To better understand the long-term temporal behavior from 1970s to present, the Noah-MP land surface model was calibrated at both soy and alfalfa sites based on RELAMPAGO data. Long-term simulation of the calibrated model suggests that ~95% of precipitation is evaporated in the alfalfa site with negligible recharge and runoff. In the case of soy, ET is about 68% of precipitation, leaving nearly 28% for recharge and 4% for runoff. Observed increases in streamflow and decreases in water table depth over time are likely linked to shifts in land cover. The changes in water table depth are enhanced in El Nino years. Furthermore, the partitioning of net radiation shifts from latent heat to sensible heat resulting in a 250% increase in Bowen ratio (from 0.2 to 0.7).

Hosted file

`wrr_si_spal.docx` available at https://authorea.com/users/532175/articles/597848-investigating-the-effects-of-land-use-change-on-subsurface-surface-and-atmospheric-branches-of-the-hydrologic-cycle-in-central-argentina

Investigating the Effects of Land Use Change on Subsurface, Surface and Atmospheric Branches of the Hydrologic Cycle in central Argentina

Sujan Pal[1], Francina Dominguez[1], Pablo Bollatti[2], Yi Yang[3], Javier Alvarez[4], Carlos Marcelo Garcia[4]

[1]Department of Atmospheric Sciences, University of Illinois at Urbana-Champaign, IL, USA.

[2]Instituto National de Technología Agropecuaria, Argentina.

[3]Department of Natural Resources and Environmental Sciences, University of Illinois at Urbana-Champaign, IL, USA.

[4]Institute for Advanced Studies for Engineering and Technology (IDIT CONICET-UNC) and Exact, Physical and Natural Sciences College, National University of Córdoba, (FCEFyN – UNC). 1611 Velez Sarsfield Ave, Córdoba, Argentina.

Corresponding author: Francina Dominguez (francina@illinois.edu)

Key Points:

- RELAMPAGO field observations and Noah-MP modeling are used to demonstrate that the fluxes of moisture and energy differ significantly between alfalfa and soy crops in central Argentina.

- Water table depth has significantly decreased, and runoff has increased over agricultural areas of central Argentina during the recent decades.

- Land cover changes partly explain regional changes in water table depth, runoff and Bowen ratio in central Argentina.

Abstract

Since the 1970s, agricultural production in central Argentina has shifted away from perennial crops and grasses towards annual crops, largely soy. In this work we use observations and modeling to understand how this shift in land cover has affected the sub-surface, surface and atmospheric fluxes of moisture and energy in a flat agricultural area. We analyze the flux tower data from a paired site at Marcos Juarez in central Argentina during the period of the RELAMPAGO field campaign (2018-2019). When compared to perennial alfalfa, the observations over soy show lower evapotranspiration and specific humidity, higher sensible heat, higher outgoing shortwave radiation and soil temperature. Furthermore, water table depth is shallower below the soy than the alfalfa sites. To better understand the long-term temporal behavior from 1970s to present, the Noah-MP land surface model was calibrated at both soy and alfalfa sites based on RELAMPAGO data. Long-term simulation of the calibrated model

36　suggests that ~95% of precipitation is evaporated in the alfalfa site with negligible recharge and
37　runoff. In the case of soy, ET is about 68% of precipitation, leaving nearly 28% for recharge and
38　4% for runoff. Observed increases in streamflow and decreases in water table depth over time are
39　likely linked to shifts in land cover. The changes in water table depth are enhanced in El Niño
40　years. Furthermore, the partitioning of net radiation shifts from latent heat to sensible heat
41　resulting in a 250% increase in Bowen ratio (from 0.2 to 0.7).

1. Introduction

43　　During the 21st century, Argentina (Figure 1a) has experienced one of the fastest agricultural
44　expansion rates in the planet (Baldi et al., 2008; Graesser et al., 2015). In many Argentinian
45　regions, such as the province of Córdoba (Figure 1b), the past 60 years have seen a shift in
46　agricultural production from one that had primarily perennial crops for livestock and grasses to
47　one based on annual crops, largely dominated by soy, with confinement of livestock into
48　feedlots. These changes came about due to a confluence of global and national factors.
49　Technological advances in agricultural production such as the introduction of transgenic
50　varieties, no-till farming, and crop rotation dramatically increased crop productivity in the region
51　(Paruelo et al., 2005). Global economic shifts such as the increasing demand of soy-based and
52　corn-based biofuels and the incursion of China, a large importer of soy-based products, into the
53　World Trade Organization made it economically attractive for farmers to shift to soy and corn.
54　At the national level, Argentinian protectionist policies of the early and mid-2000s significantly
55　benefited the agricultural industry. As a result, in two decades (1995/96 to 2014/15), the
56　cultivated area in regions such as Córdoba increased by 229%. Soy now dominates the landscape
57　in the province of Cordoba accounting for nearly 60% of crops.

58　　How can these dramatic changes in land use affect the hydrologic cycle? Some effects could
59　parallel those of other regions of the globe that have experienced similar land use shifts, such as
60　the Midwestern United States. In the US central region, European settlers arrived in the early to
61　mid-19th century and by 1900 agriculture had become the dominant land use type, replacing the
62　native grasses and forests of the region (Yaeger et al., 2013). Perennial and sod vegetation gave
63　way to intensive corn and/or soybean crops with shorter summer growing seasons, which led to a
64　decrease in evapotranspiration (ET). Decreased ET implied that more precipitation was going
65　into groundwater recharge and routed into streams as baseflow (Zhang and Schilling, 2006).
66　Furthermore, the ubiquitous use of tile drainage accelerates the lateral subsurface drainage of
67　these systems (Yaeger et al., 2013). Several studies have attributed increased baseflow in the
68　region to changes in land surface characteristics (Zhang and Schilling, 2006; Schilling et al.,
69　2008; 2010; Xu et al., 2013).

70　　The plains of the Pampas-Chaco in Argentina are flatter than their North American
71　counterparts. They are sometimes referred to as hyperplanes, because their slopes are less than
72　0.1%, their drainage systems are poorly developed, and ET dominates the water balance
73　(Jobbagy et al., 2008). Rodriguez et al., 2020 identified transpiration as the primary component
74　of the water budget, followed by ET and interception, for dry forests and crops in the nearby
75　region of San Luis. In general, their modeling results showed that liquid water fluxes here are
76　strongly controlled by the vegetation cover. Giménez et al., 2020 illustrated that changes in land

77 cover from dry forests to crop reduced ET and increased intensity of deep drainage.
78 Consequently, changes in ET linked to agricultural practices can have dramatic consequences in
79 the water balance of the region. Measurements and remote-sensing estimates in Argentina show
80 that compared to annual crops,
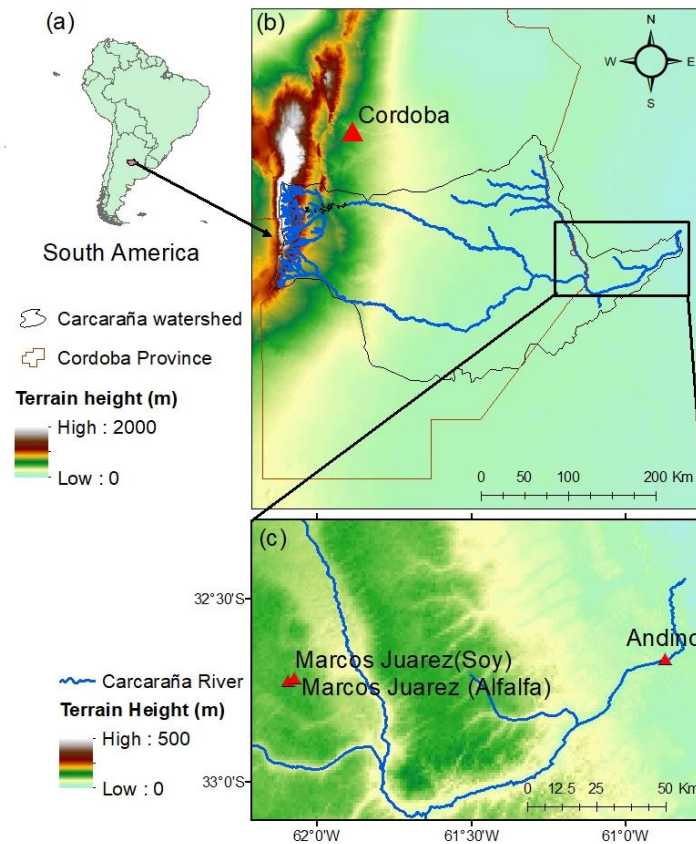
81

82 **Figure 1.** (a) Location of Carcarañá river basin in Argentina. (b) Elevation (m) and drainage
83 network of the basin. (c) Location of Marcos Juarez (paired sites) and Andino (streamflow
84 measurement location) within the watershed.

85 perennial crops such as alfalfa have deeper roots and year-round transpiration of more than 1000
86 mm/year compared to about 680 mm/year for single summer crops (Nosetto et al., 2015). Soil
87 moisture is usually higher, and the water table depth is closer to the surface below annual single
88 summer crops than in areas where perennial alfalfa is grown (Nosetto et al., 2012). Mercau et al.
89 (2015) suggests that at inter-annual timescales, the balance between precipitation and ET dictates
90 water table fluctuations, whereas crop choice can be a relevant control at intra-annual or seasonal
91 timescale. They also indicated that lateral transport of water, driven by hydraulic gradients
92 develops due to contrasting water consumption of different vegetation types. In a modeling study
93 Zellner et al. (2020) reach a similar conclusion, as climate was the main driver of water table
94 dynamics, but crops can influence water levels depending on the growing cycle. One of the

95 important consequences of changes in water table is related to flooding, as groundwater level is
96 intimately related to the flooded area in the region (Viglizzo et al., 2009; Aragón et al., 2010).
97 During periods of excess rains, the water table can reach the surface and cause "slow" floods that
98 affect the region for several years (Kuppel et al., 2015). In fact, a modeling study by Lee et al.,
99 2018 linked the increasing discharge of Parana river to land cover change using a terrestrial
100 biosphere model.

101   Very few studies have relied on eddy covariance data in this region due to limited in-situ
102 measurements. Garcia et al., 2017a provided estimates of CO_2 and water vapor fluxes, using
103 eddy covariance measurements, in a dry forest of central Argentina. They identified that (1) the
104 dry forest is a net sink of carbon, and (2) ET is the dominant vapor flux. In another study,
105 Nosetto et al. (2020) compared the temporal patterns of CO_2 and water vapor fluxes of native dry
106 forests and pastures at two different locations to show comparatively higher ET in the forests,
107 primarily due to increased evaporating surface causing higher intercepted water. Long-term
108 ground water table depth records are also limited in this region. Jobbágy et al., 2020 illustrated
109 that unsaturated-saturated contact zone is a critical and dynamic hub of water partition using
110 observed water table depth analysis at different vegetation. Clearly, this region shows strong
111 interactions between land cover and terrestrial hydrology. However, there have not yet been any
112 paired hydrometeorological observations of eddy-covariance estimates in the region, to
113 understand how transient changes in land cover affect the partitioning of moisture and energy.
114 Furthermore, the link between these differences and long-term trends in water table depth,
115 hydrologic and atmospheric fluxes has not been established.

116   This study focuses on the regions surrounding Marcos Juarez (Figure 1c), a town located in
117 the Carcarañá river basin in the Pampas region of Argentina, in central-southeast of Córdoba
118 province. This region has experienced a dramatic transformation from mostly perennial grasses
119 and alfalfa to annual (mostly soybean) cultivation (Figure 2) and is representative of the land-use
120 changes in the region as a whole. Critically, the Argentinian National Institute for Agricultural
121 Technology (INTA, for its acronym in Spanish) has an experimental alfalfa site and several soy
122 sites in this location. Alfalfa is a perennial crop with characteristics similar to those that would
123 have dominated the landscape in the 1970s, and soy crops are representative of the region at
124 present. In addition, INTA has long-term water table depth observations (see section 2.1 and
125 3.1). We deployed two eddy covariance towers within the INTA site as part of the
126 RELAMPAGO (Remote Sensing of Electrification, Lightning and Mesoscale/ Microscale
127 Processes with Adaptive Ground Observations) field campaign which took place in west central
128 Argentina (Nesbitt et al., 2016; Pal et al., 2021). The RELAMPAGO project consisted of an
129 Extended Hydrometeorology Observing Period (EHOP) from 1 June 2018 to 30 April 2019. One
130 of the goals of the EHOP is to understand how changes in land cover have affected the
131 partitioning of rainfall between infiltration/runoff and impacted the residence times of soil
132 moisture and groundwater in the Carcarañá Basin's terrestrial system. As part of the EHOP, the
133 hydrometeorology team of RELAMPAGO installed thirty meteorological stations, including
134 seven eddy covariance towers. The work we present in this manuscript is based on the two eddy
135 covariance towers located within the INTA experimental site in Marcos Juarez Argentina (Figure
136 1).

137
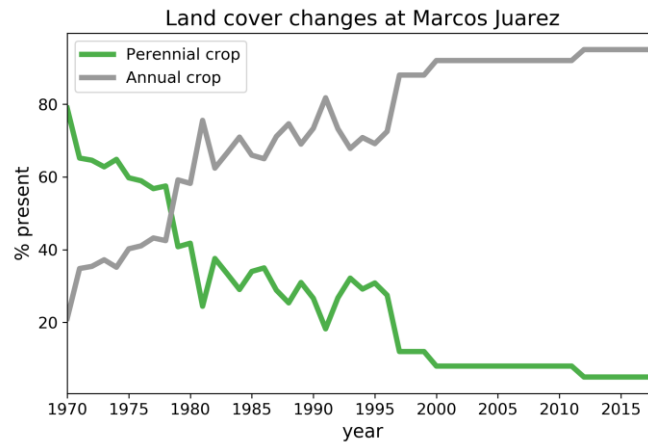
Figure 2. Evolution of land use change in Marcos Juarez, also representative of a large region of Argentina.

The goals of this manuscript are (1) to quantify the differences in energy and moisture fluxes between soy and alfalfa using high-resolution intra daily eddy covariance observations obtained from two RELAMPAGO flux towers, and (2) to understand the long-term effects of the gradual long-term shift from perennial to annual crops on surface, subsurface and atmospheric hydrology of the region with the help of a land surface model. The results from this study can be used to interpret long-term ET estimates in this region, which are also useful for INTA. Critically, the results from this study have implications for interpreting changes in water table depth based on land cover type and climate variability (such as El Niño and La Niña conditions). It is organized as follows: in section 2, the description of observed data, model specifications and the experimental design are discussed. In Section 3, the results are discussed and finally, the conclusions are summarized in Section 4. Additional information is provided in the Supporting Information (SI).

2. Materials and Methods

2.1 Long-term observations

Long-term measurements (1970-2020) of annual mean water table depth, precipitation and temperature were obtained from the agrometeorological station of the INTA Marcos Juárez. Annual runoff measurement from 1980 -2020 was obtained from the streamflow station at Andino (Figure 1c). The Carcarañá river drains an area of 60,000 km^2 at Andino (60.87W, 32.67S), which has long-term daily discharge information (Source: National Secretary of Water Resources). As such, Andino is downstream of Marcos Juarez as well as most of the Carcarañá river basin. Total runoff at Andino was further separated into baseflow and surface flow using Web-based Hydrograph Analysis Tool (WHAT) recursive digital filter method (Eckhardt, 2012). Throughout the text, significance is assessed using the Mann Kendall trend test at 95% significance level. Sequential Mann Kendall test (Sneyers, 1990; Modarres and Sarhadi, 2009) was used to detect breakpoints in discharge (see Figure S1 in SI).

2.2 RELAMPAGO 10-month observations

166   To understand the effect of different land use types on the fluxes of energy, moisture and
167   momentum along the subsurface-surface and atmosphere continuum, the RELAMPAGO
168   Hydrometeorology team installed two eddy covariance towers within the INTA experimental
169   station in Marcos Juarez (Figure 1c). One of the towers was located within an alfalfa test plot
170   (62° 4.492'W, 32° 42.970'S), while the other one was located in a soy site (62° 5.085'W, 32°
171   43.518'S; Figure 1c). RELAMPAGO flux measurements are part of the Integrated Surface Flux
172   System (ISFS) (https://www.eol.ucar.edu/content/isfs-operations-relampago) maintained by the
173   National Center for Atmospheric Research (NCAR) Earth Observing Laboratory (EOL). 3-D
174   sonic anemometers and H_2O/CO_2 gas analyzers were used to measure net evapotranspiration and
175   surface energy balance. As such, the sensible and latent heat fluxes were obtained from sonic
176   anemometer measurements of vertical velocity, temperature and fast-response hygrometer
177   measurements of water vapor density. Soil moisture sensors were installed at 5 cm depth.
178   Radiation measurements were derived from the radiometers.

179   For this study, we analyze soil moisture (SM), sensible (SHF), latent heat fluxes (LHF,
180   measured by the eddy covariance method), specific humidity (SH), outgoing shortwave radiation
181   (OSR), soil temperature (ST), 2-m temperature (T2m), momentum in zonal and meridional
182   direction (U- and V-momentum), and incoming shortwave radiation (ISR). The flux tower
183   measurements were available from June 1, 2018 to April 1, 2019. However, good quality soil
184   moisture data was only available from November 2018 to March 2019. Continuous groundwater
185   measurements were obtained in the soy and alfalfa sites from both automated sensors and manual
186   extraction by INTA and data was available from July 2018 to May 2019.

187   Our observations include the full crop planting-harvesting cycle. In Argentina, soy planting
188   begins in September-October and planting ends in November, during the months of austral
189   spring. December-February is the growing season (austral summer), and harvesting begins in
190   March. Harvesting is completed by April-May. During the austral winter months, cover crops are
191   sometimes planted to improve soil fertility and quality, as they were during the 2018-2019
192   season in Marcos Juarez.

193   *2.3 Land surface modeling with Noah-MP*

194   Land surface models compute the exchanges of water, heat, radiation and momentum between
195   the land and atmosphere (Sellers et al., 1997; Zheng et al., 2019). In this study we use the Noah
196   LSM (Chen and Dudhia, 2001) with multi-parameterization options (Noah-MP; Niu et al. 2011)
197   run in a column (one-dimensional in the horizontal direction) configuration. Noah-MP calculates
198   energy, water, and carbon dioxide fluxes between the biosphere and the atmosphere for different
199   vegetation types, with closed energy budget and coupled water cycle. It has been previously
200   implemented to investigate problems related to hydrologic cycle in standalone mode (Cai et al.,
201   2014; Martinez et al. 2016a) and coupled with WRF (Martinez et al., 2016b; Pal et al., 2019) or
202   WRF-Hydro (Gochis et al., 2018; Pal et al., 2021).

203   We use the Noah-MP land surface model in 'offline' mode with a groundwater scheme (Niu et
204   al. 2007) to better understand the physical processes in the two sites with different vegetation and
205   evaluate these processes for periods when we do not have observations (Figure 3a). The Ball-

206   Berry scheme was chosen for modeling stomatal resistance. Other parameterizations of Noah-
207   MP were left as default; such as Monin-Obukhov scheme for surface layer drag, Jordan scheme
208   for partitioning precipitation into rainfall and snowfall etc. (Niu et al., 2011). We do not analyze
209   carbon fluxes in this work, so the carbon and dynamic vegetation module was not used. In the
210   model, vegetation is represented by generic plant functional types, so the model needs to be
211   calibrated regionally for best results. To better represent the soil state and ground water-soil
212   moisture interaction, we modified the model soil column to have 14 layers (Table S1 in SI)
213   extending from the surface to 4m below (following Miguez-Macho and Fan, 2012; Martinez et
214   al., 2016a) while the default Noah-MP has only 2m deep soil column (with 4 layers).

215
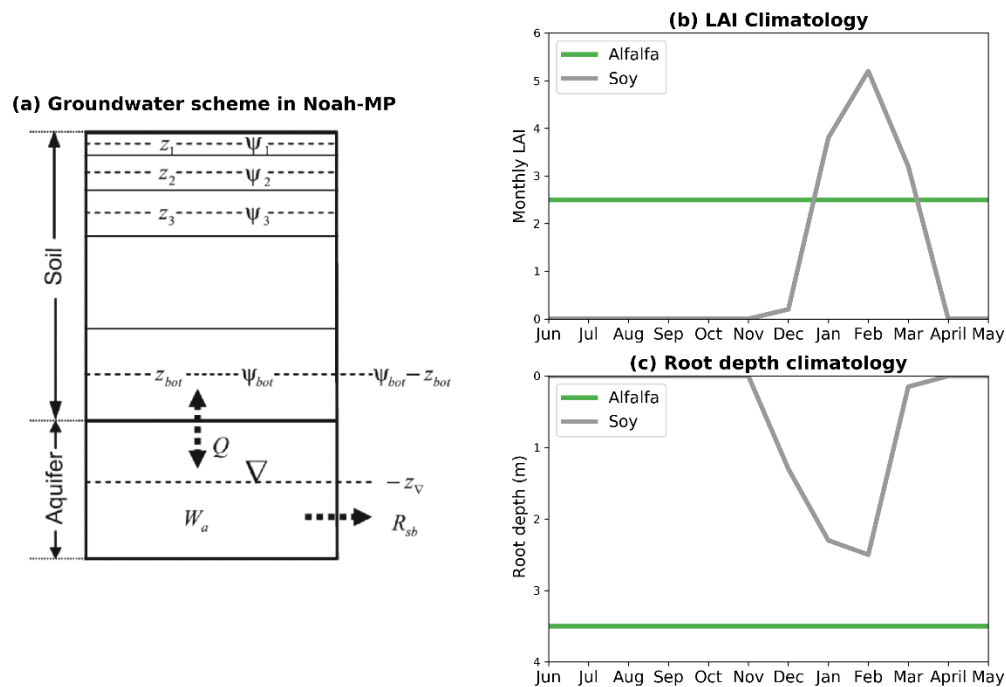
Figure 3. (a) Noah-MP groundwater model structure (adapted from Niu et al., 2007), z_i = height
of soil layers, ψ = water head, Q = recharge rate (mms^{-1}), z_∇ = water table, bot = bottom layer,
W_a = water stored in the aquifer (mm), R_{sb} = subsurface discharge (mms^{-1}), (b) LAI and (c) Root
depth climatology used in the model simulation for Soy and alfalfa.

220   The model is run with prescribed atmospheric conditions from Global Land Data Assimilation
221   System (GLDAS; Rodell et al., 2004) extracted for Marcos Juarez (nearest grid point from
222   GLDAS). First, we performed two independent experiments named 'Noah-MP SOY' and 'Noah-
223   MP ALFALFA' where the model configuration remains unchanged except for the vegetation
224   parameters in the model. The vegetation parameters varied depending on the type of crop were 1)
225   leaf area index (LAI), 2) root depth (RD), 3) maximum carboxylation rate (VMAX) in the
226   Farquhar photosynthesis model (Farquhar et al., 1980), 4) the slope parameter (MP) and 5) the

227   intercept parameter (BP) in the Ball-Berry stomatal conductance model (Ball et al., 1987).
228   VMAX, BP and MP controls the ET by controlling the stomatal resistance ($r_{s,i}$).

$$\frac{1}{r_{s,i}} = MP\,\frac{A}{c_{air}}\,\frac{e_{air}}{e_{sat}(T_v)}P_{air} + BP$$

229   Where 'A' is photosynthesis rates per unit LAI of leaves, which is controlled by VMAX. C_{air} is
230   the CO_2 concentration at leaf surface, P_{air} is the surface air pressure. E_{air} and e_{sat} are vapor
231   pressure at leaf surface and saturation vapor pressure at leaf surface temperature, respectively.
232   Simulated ET is highly sensitive to these parameters of Noah-MP (Cuntz et al., 2016). Other
233   vegetation parameters (e.g. leaf reflectivity, stem reflectivity, vegetation height, height of lower
234   canopy bound etc.) for the Noah-MP ALFALFA and Noah-MP SOY simulations were kept as
235   default Noah-MP values of 'Grasslands' and 'Croplands' modified IGBP MODIS 20-category
236   vegetation, respectively. The soil type was taken as silty clay loam for both the sites.

237   The climatology of LAI and RD for the two vegetation types were obtained from literature
238   (Figure 2 of Garcia et al. 2017b). Alfalfa grows during the whole year and have a deeper root
239   system (3.5 m), while soy crops occupy the field only 4-5 months. In Noah-MP, we provided the
240   root depth monthly climatology and prescribed monthly LAI climatology (Figure 3b, 3c) from
241   Garcia et al., 2017b. As such, we did not use dynamic root or dynamic vegetation calculations.
242   There are some remotely sensed LAI products available in this region, but they do not accurately
243   represent the LAI climatology of these two specific vegetations, so we relied on this local
244   literature reported LAI estimates. The two short-term simulations Noah-MP ALFALFA and
245   Noah-MP SOY were performed to calibrate and validate the model at the two sites (see section
246   2.3.1 and section 3.3). The complete list of modeling experiments is presented in Table 1.

247   **Table 1.** List of experiments performed in this study.

Name of simulation	Simulation period	Vegetation	Forcing	Purpose
Noah-MP ALFALFA	June 1, 2018 – April 1, 2019	100% alfalfa	GLDAS	Calibration and validation
Noah-MP SOY	June 1, 2018 – April 1, 2019	100% soy	GLDAS	Calibration and validation
Noah-MP ALFALFA LT	January 1, 1970- December 31, 2018	100% alfalfa	GLDAS	Long term estimates of water budget and surface fluxes
Noah-MP SOY LT	January 1, 1970- December 31, 2018	100% soy	GLDAS	Long term estimates of water budget and surface fluxes

248

249   Using the calibrated model (see section 2.3.1) we performed two long-term simulations for
250   100% alfalfa and 100% soy conditions for the period January 1970 – April 2019 (Noah-MP
251   ALFALFA LT and Noah-MP SOY LT, respectively in Table 1). The calibrated parameters for

252 the two vegetation types are used in the long-term simulations, and the GLDAS forcing for 1970-
253 2019 is used to capture the interannual variability of the model inputs. These simulations provide
254 components of annual water budget in the two different vegetation scenarios. It is worth
255 mentioning here that these two scenarios are the two extremes of land use, and the actual
256 transient land use would fall somewhere in between. However, this kind of experiment helps us
257 understand the possible largest extent of transformation in hydrology due to land use change in
258 this region. In our modeling experiment we do not take into account the effect of lateral flow
259 (which might be generated by heterogeneous land cover) at inter-annual time scale. We spin up
260 the model for 40 years for both scenarios and use the final SM and water table depth as the initial
261 condition for the analyzed simulations.

2.3.1. Calibration

263 In Noah-MP, ET is most sensitive to the vegetation parameters VMAX, BP and MP (Cuntz et
264 al., 2016). So, these parameters were obtained by calibration of the model based on
265 RELAMPAGO flux tower observations of daily LHF at both the sites. All other parameters of
266 the model were kept constant as the default configuration (section 2.3). The calibration was
267 performed in a shuffle complex evolution method (Duan et al., 1993) minimizing the root mean
268 square error (RMSE) of daily LHF data. Python SPOTPY package (Houska et al., 2015) was
269 used to carry out the calibration. By this method, we can make realistic estimates of land surface
270 variables at these two sites using Noah-MP (which previously had default generic crop
271 parameters). The model was calibrated separately with respect to daily LHF data at both the sites
272 to obtain the above-mentioned vegetation parameters. It is worth remembering here that our main
273 goal from these modeling exercises is to obtain realistic water and energy balances for these two
274 types of vegetations. LHF is a major part of both energy and water balance (as ET). Hence, we
275 preferred to calibrate the model based on the common link (ET) of these two budget equations.
276 The model was validated on the other variables during the same time period (June 1, 2018 –
277 April 1, 2019) at those sites.

278 The results of calibration and validation is included in Table 2. For the soy (alfalfa) site, the
279 parameters found were: VMAX = 132.425 (136.734), BP = 1580.63 (2041), MP = 6.89 (5.95).
280 The model performance was validated against SHF and SM, at daily scale, at both the sites. The
281 performance was significantly improved from the default parameter combinations, which
282 underestimated the latent heat fluxes at both the sites. These calibrated parameters were used in
283 the long-term simulations Noah-MP ALFALFA LT and Noah-MP SOY LT.

3. Results

3.1 Analysis of Long-Term Data

286 In 1970, the water table was nearly 11 m deep, however there has been a steady rise
287 (statistically significant decreasing trend) of the water table and now it is approximately 2 m
288 below ground at Marcos Juarez (Figure 4a). This trend does not seem to be related to climatic
289 variables, e.g., precipitation and temperature. Annual mean precipitation shows a slight
290 statistically non- significant decreasing trend (Figure 4b) and annual mean temperature shows a
291 statistically

Table 2. Calibration and validation of Noah-MP at daily scale at the two sites. CC = correlation coefficient, RMSE = root mean square error.

		Alfalfa site		Soy site	
		CC	**RMSE**	**CC**	**RMSE**
Calibration	**Latent heat flux**	0.78	32.61	0.65	37.45
Validation	**Sensible heat flux**	0.62	24.62	0.64	20.1
	Top layer soil moisture	0.57	17.56	0.49	17.74

significant increasing trend (Figure 4c).
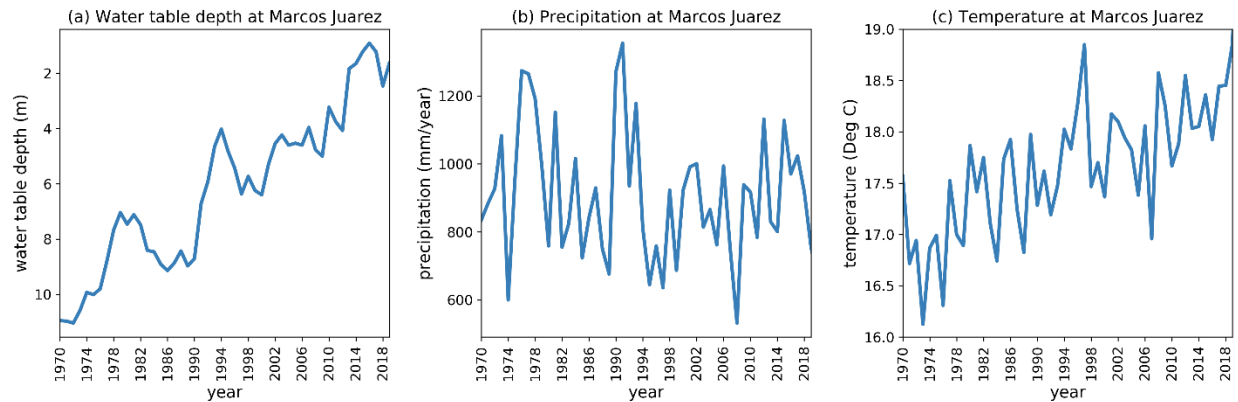
Figure 4. Long-term timeseries of annual mean (a) water table depth, (b) precipitation and (c) temperature at Marcos Juarez based on the Agrometeorological Station of the INTA Marcos Juárez and manual water table depth observations.

Streamflow at Andino has a statistically significant increasing trend, especially after 2000 (Figure 5). The increasing trend in total flow is result of both increased baseflow (statistically significant trend) and surface flow (statistically non-significant trend, Figure 5a). The year 2000 was found to be a year of change-point of trend (sequential Man-Kendall test, Figure S1 in SI). After 2000, baseflow has increased in the months of March and April; whereas surface flow has increased remarkably in February, March and October (Figure 5b). The combined effect of surface runoff and baseflow has resulted in the overall increase in streamflow at the Andino gauging station (Figure 5b-Figure 5d).

3.2 Analysis of the RELAMPAGO data

The analysis of the RELAMPAGO flux towers data is limited to the period June 1, 2018 to April 1, 2019 which corresponds to the EHOP. Figure 6 presents values at (1) sub-daily, (2) daily and (3) monthly timescale.

Hourly fluxes of sensible and latent heat in the soy and the alfalfa site show different characteristics. Diurnal cycles of LHF and SHF at both sites peak around 16 UTC (1 PM local

314   time, Figure 6a, 6d). The difference in magnitude is nominal at nighttime, and it increases during
315   daytime. During most months, LHF (SHF) was higher at the alfalfa (soy) site than in the soy
316   (alfalfa) site. The highest differences in the diurnal cycles of LHF (SHF) is found in December


317
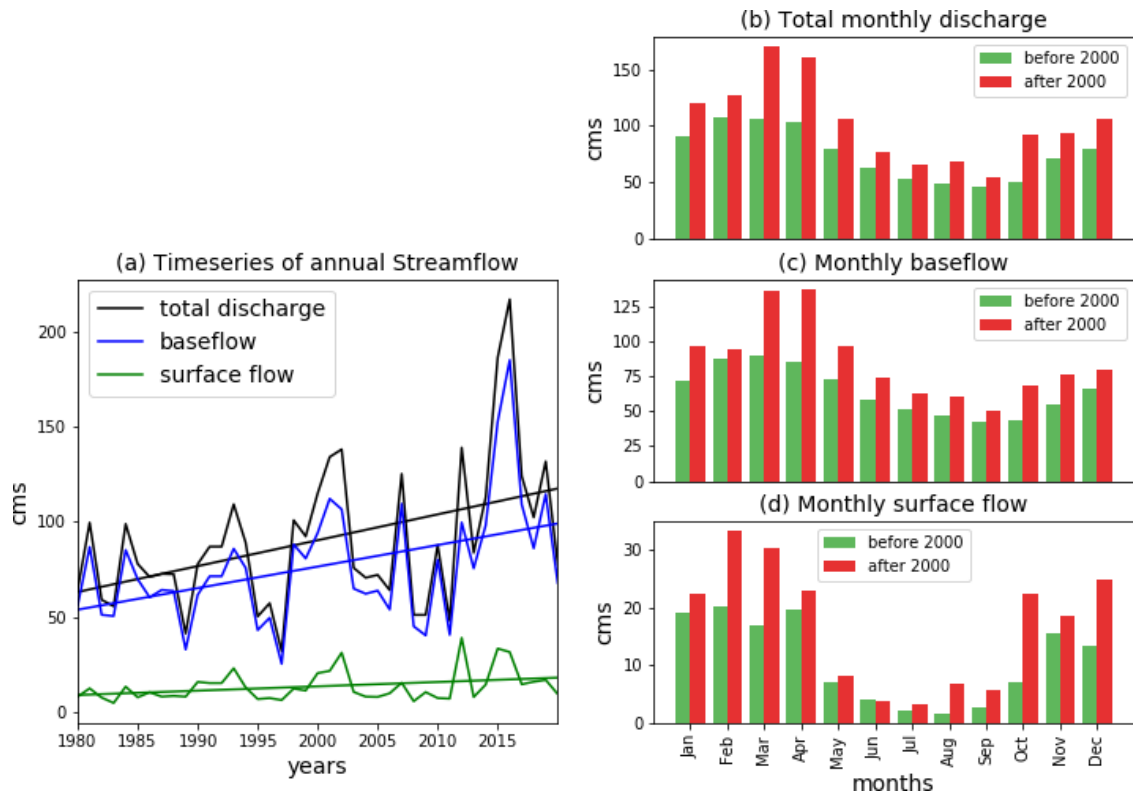
Figure 5. (a) Annual mean streamflow at Andino 1980-2016. Linear fit lines (solid straight lines)
are also included. Monthly mean streamflow before and after 2000 separated into (b) total, (c)
baseflow and (d) surface flow. cms = cubic meter per second.

321   (October). Sub-daily values of LHF (SHF) are comparable in the months of January and March
322   (February and March). (2) Daily values of LHF are higher for alfalfa during most of the year,
323   except for January, February and March, which correspond to the peak of the soy growing
324   season when the annual crops are transpiring vigorously (Figure 6b and 6e). Daily values of SHF
325   are much higher for Soy in all months, except February (Figure 6e). (3) Monthly mean values
326   reinforce these facts (Figure 6c, 6f). LHF for alfalfa (soy) peaks in December (January). SHF for
327   alfalfa (soy) peaks in February (December). This is related to the phenology of crops in this
328   region (see section 2.2 and Figure 3b-3c). Crops transpire most during the end of growing season
329   when they are mature. At the beginning of growing season, sensible heat is maximized. Based on
330   our eddy covariance measurements, the accumulated 10-month ET of soy was found to be
331   approximately 550 mm while for alfalfa it was around 880 mm.

332   In addition to sensible and latent heat, we analyzed specific humidity (SH), outgoing
333   shortwave radiation (OSR), soil temperature (ST), T2m, U- and V-momentum and incoming
334   shortwave radiation (ISR) measurements from the two sites. SH is higher at the Alfalfa site in all
335   months except February and March at sub-daily, daily and monthly scale (Figure 7a-7c). The

difference is largest in January. This indicates that the atmosphere above alfalfa is more humid due to higher transpiration of the plants. OSR is higher at the Soy site in all months (Figure 7d-7f). This is likely related to higher albedo of Soy when compared to Alfalfa. This radiative effect alters the net incoming solar radiation. Soil temperature is higher at the Soy site in all months, except January and February (Figure 7g-7i), and this is linked to the higher SHF in the soy plot (Figure 6d-6f). No significant difference was found for T2m, U- and V-momentum and ISR (not shown). This indicates that thermodynamic properties are altered by the change in vegetation, but not the dynamic properties.

Water table is shallower at the soy site (Figure 8) by more than 1 meter and this difference increases in summer months when we see a sharp increase in water table following the first rains (November- February). We also see that the automated water table depth measurements (continuous line) agree with the manual observations (points). It is worth mentioning here that these measurements are critical in this region, as satellite estimates like GRACE fail to show the variation in water table depth (Figure S2 in SI), most likely due to its coarse resolution.
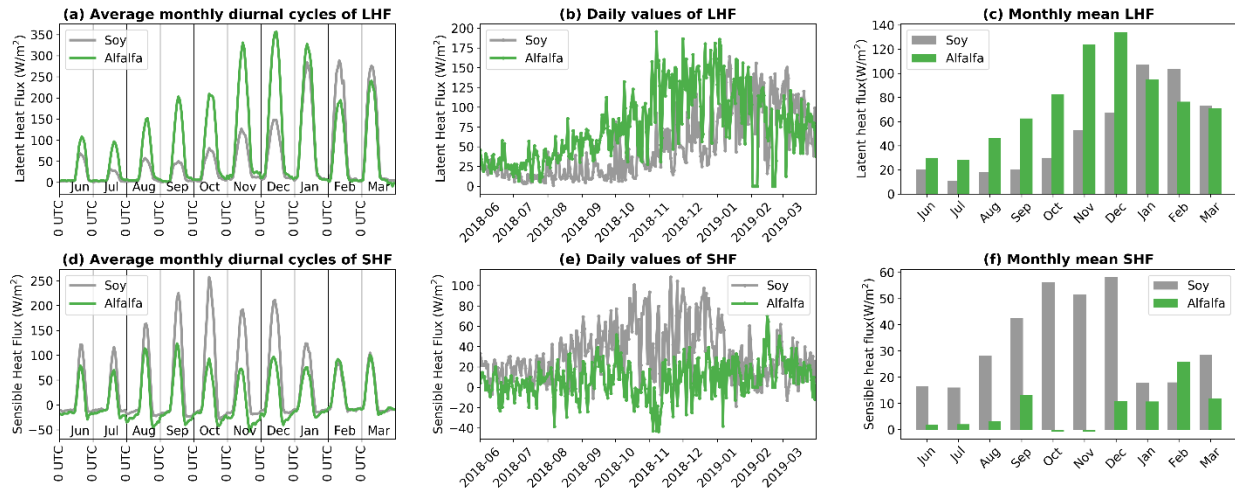
Figure 6. Diurnal, daily and monthly values of latent (a, b, c) and sensible heat flux (d, e, f) respectively at Marcos Juarez as observed by EOL towers during RELAMPAGO.

3.3 Model validation

When compared to observations, the Noah-MP calibrated model performs realistically for both the sites (Figure 9). LHF at the soy site was well represented by the model, except for some high daily values in October and December (Figure 9a). LHF at the alfalfa site was slightly underestimated during some days in the Spring and overestimated in the Summer months (Figure 9b). SHF was slightly underestimated by Noah-MP at the soy site and overestimated at the alfalfa site (Figure 9c, 9d). The model does a reasonable job (Figure 9e, 9f) in simulating the top layer SM (0-5cm), unfortunately we do not have SM observations until November of 2018. The discrepancies between model simulated fluxes and observations can be attributed to the simple structure of the Noah-MP model and calibration of limited variables within the model. Noah-MP assumes uniform soil with depth, uniform root distribution throughout the soil layers, ignores hydrologic redistribution which can play a role in modifying the amounts of SHF and LHF.

365   However, for the purposes of this study we are interested in comparing the representation of the
366   two different vegetation types to understand the long-term effect of such changes in the fluxes of
367   energy and moisture. Also, realistic land surface modeling complements the observations in
368   terms of gap filling of missing values, which are common in these types of measurements.

369
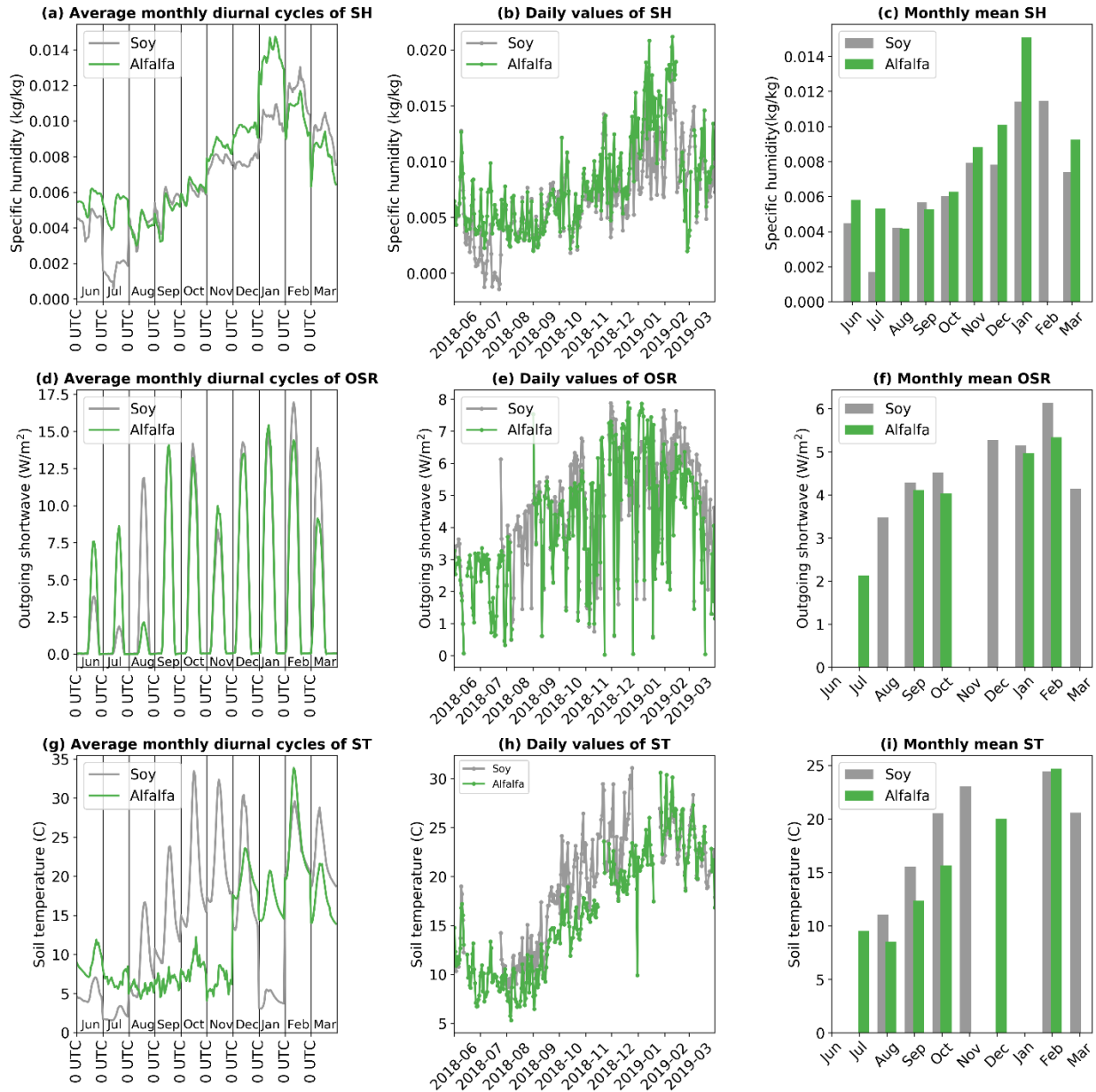
Figure 7. Diurnal, daily and monthly values of specific humidity (a, b, c), outgoing shortwave
radiation (d, e, f) and soil temperature (g, h, i) respectively at Marcos Juarez as observed by EOL
towers during RELAMPAGO.

374
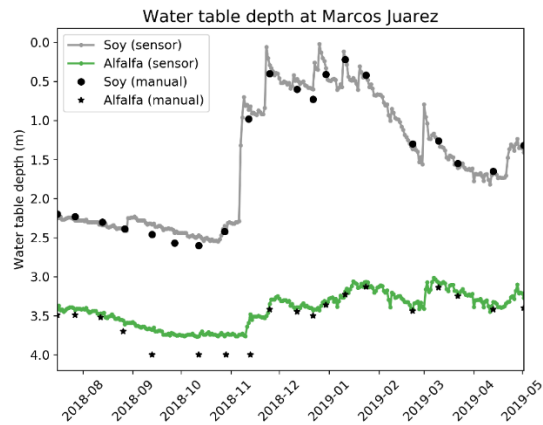
Figure 8. Water table depth at Marcos Juarez as measured by INTA during RELAMPAGO period.

377
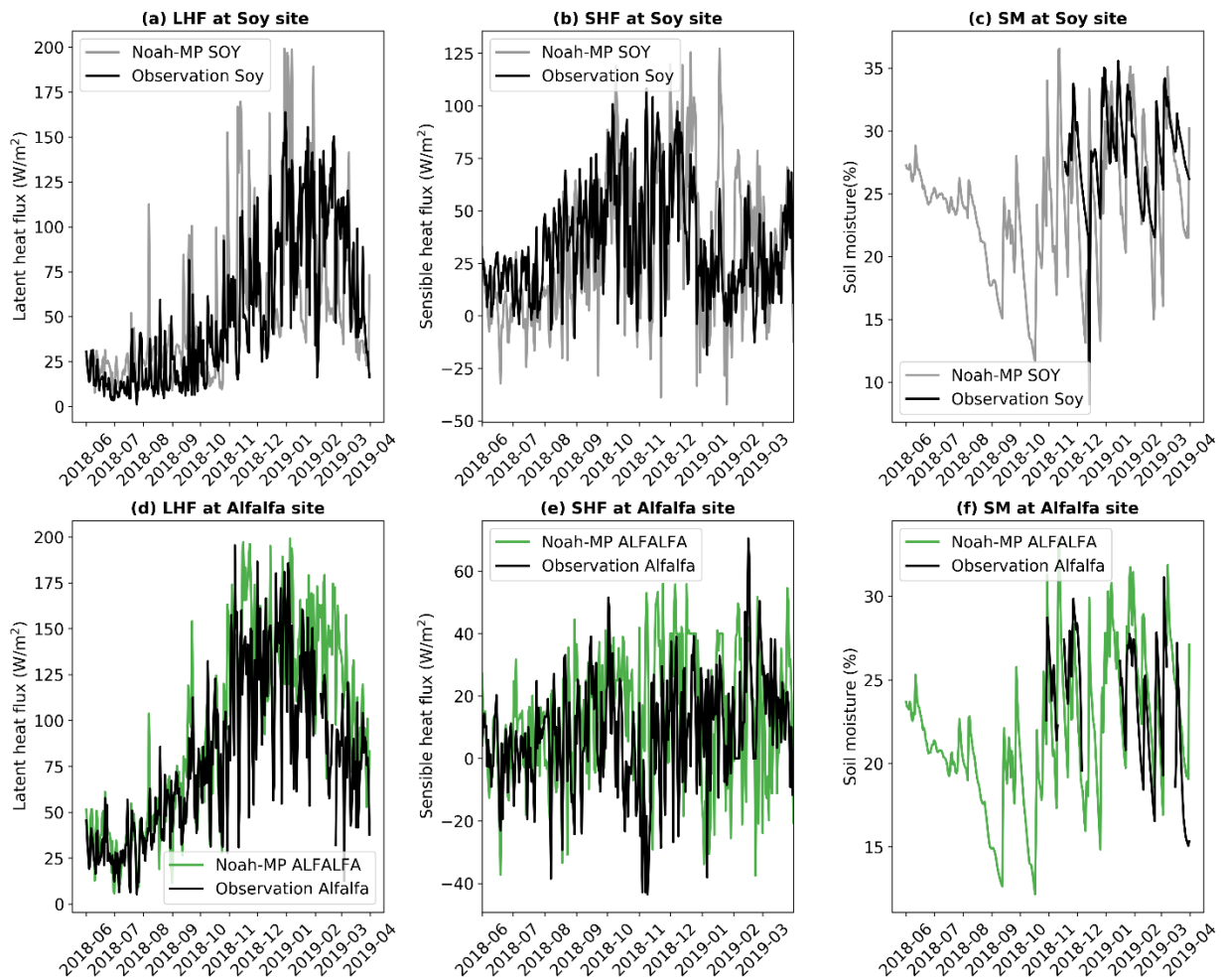
Figure 9. Calibrated Noah-MP model output at soy (a, b, c) and alfalfa site (d, e, f) as compared with EOL flux tower observation during RELAMPAGO period. Missing/ unusual soil moisture data is omitted from the plots.

3.4 Long-term water and energy balance of the two experiments

To understand how changes in agricultural practices might have changed the fluxes of water and energy, we performed two idealized long-term Noah-MP simulations for the period 1970-2018. In one simulation we set the land cover as soy (Noah-MP SOY LT, Table 1), while in the other simulation was alfalfa (Noah-MP ALFALFA LT, Table 1). Both simulations have the same atmospheric forcing for the 49-year period. The annual mean values of different components of the water budget (P = ET + R+ SR, where P = precipitation, ET = evapotranspiration, R = Recharge, SR = surface runoff, ignoring storage) of the two simulations are shown in Figure 10.

At the Alfalfa site, long-term average water balance reveals that ET is the dominant component (Figure 10a). Most of the incoming precipitation is evaporated (94.5%). Little goes into the aquifer as recharge (4.6%), along with negligible surface runoff (0.9%). This kind of partitioning of precipitation is realistic in this region (Rodriguez et al., 2020; Giménez et al., 2020). This is due to high evaporative potential of alfalfa, adequate water availability, and flatness of the region which results in very little surface runoff. The partitioning of incoming precipitation is different at the soy site (Figure 10b). In this case, a significant amount of precipitated water goes into aquifer as recharge (28.4%). This is a result of significantly less evaporation at the soy site (68.1%), when compared to alfalfa. The surface runoff component at the soy site is slightly higher (3.5%), but still negligible compared to the evaporation and recharge.

Hence, changing pasture to cropland results in four-fold increase in runoff and six-fold increase in deep recharge. These results are consistent with previous literature and observations (Nosetto et al, 2015; Rodriguez et al., 2020). The change in land use in this region results in more recharge, which contributes to a shallower water table depth and higher baseflow observed in recent years (Figure 3 and Figure 4). In other words, the moisture that would have entered the atmosphere in alfalfa vegetated region, is being accumulated below ground due to the shift in land use to soy. This shift in regime transforms the subsurface hydrology in terms of water table depth, baseflow and SM.

Analyzing the partitioning of available energy defined as the summation of latent heat flux (LHF) and sensible heat flux (SHF (Shuttleworth 1993), we find that LHF is the dominant surface flux component in both the vegetations (Figure 11). However, the balance is significantly different when comparing alfalfa and soy. LHF accounts for 85% of available energy over alfalfa while it accounts for 59% over soy. On the other hand, the 15% of the available energy over alfalfa goes into SHF, while it is 41% over soy. The Bowen ratio ($\frac{SHF}{LHF}$) reiterates this fact with mean of 0.2 over alfalfa and 0.7 over soy. Interestingly, there is a statistically significant increasing trend in Bowen ratio in the Noah-MP SOY LT simulation (p = 0.014), which is consistent with Zeng et al. 2020, and indicates a possible global warming signature further enhanced by agriculture. In other words, the recent atmosphere is having a significantly higher sensible heat flux in the spring and summer months, compared to previous decades and this is highlighted only in the soy simulation. This could also have a potential impact on the overlying

421   atmosphere, given this region is characterized by strong land-atmosphere coupling (Ruscica et
422   al., 2015).

423
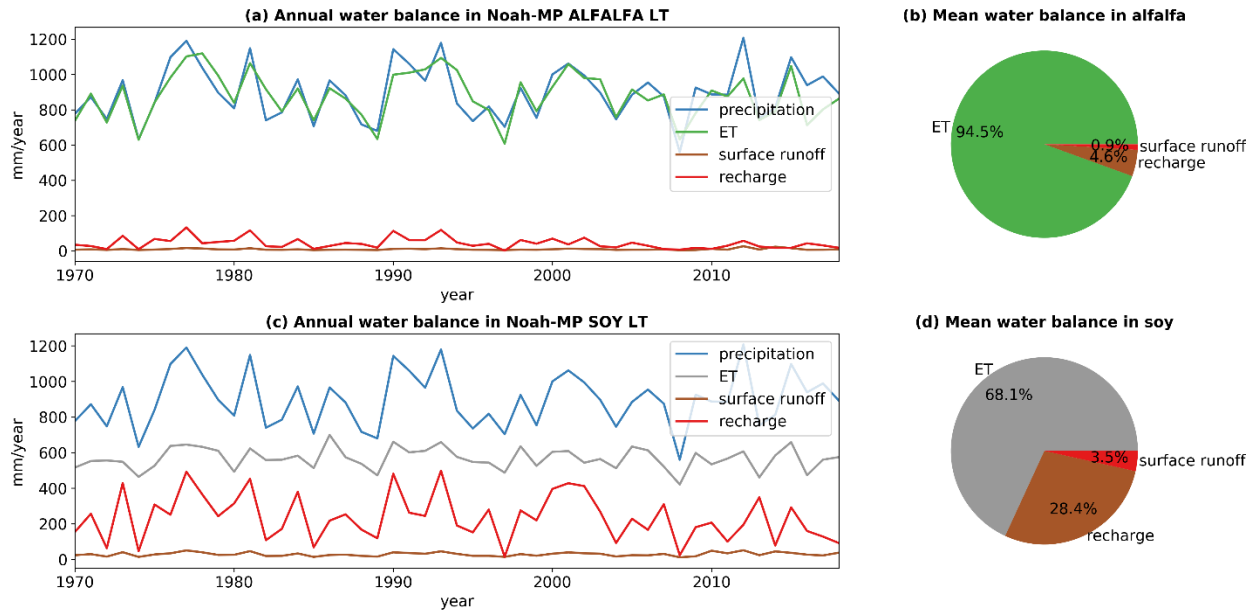
Figure 10. Long term annual estimates of precipitation, ET, runoff and recharge in (a) 100%
alfalfa and (c) 100% soy simulations. Average partitioning of water in (b) alfalfa and (d) soy as
calculated over the period 1970-2018.

427
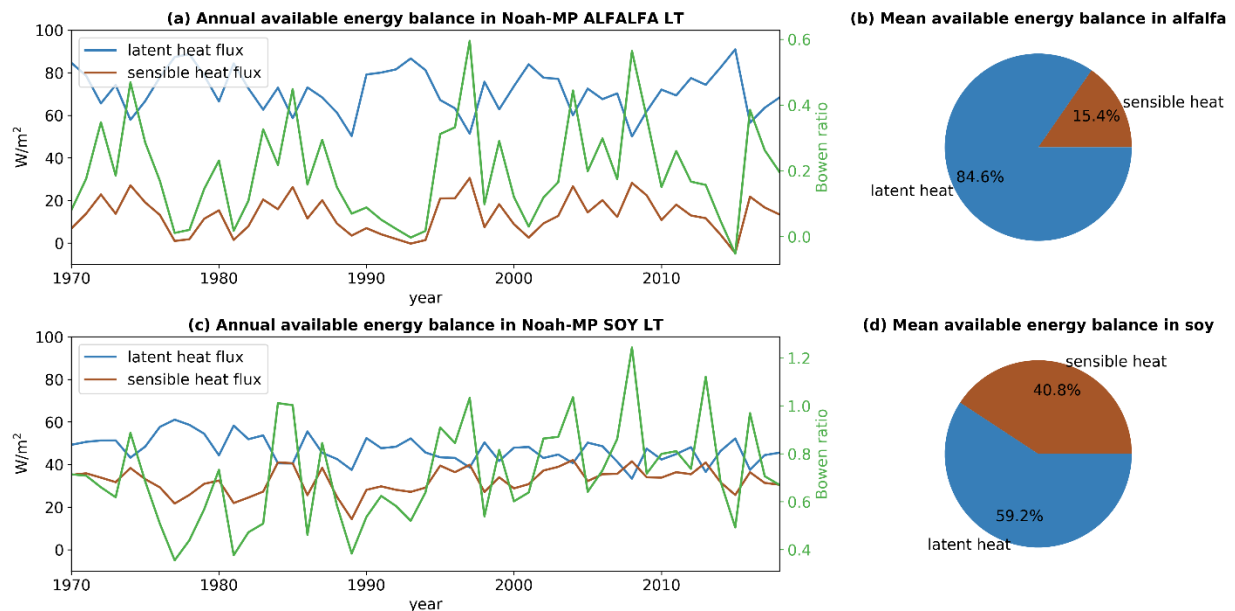
Figure 11. Long term annual estimates of LHF and SHF in (a) 100% alfalfa and (c) 100% soy
simulations. Bowen ratio is shown with green line (secondary axis). Average partitioning of
available energy in (b) alfalfa and (d) soy as calculated over the period 1970-2018.

431   *3.5. Idealized transient land cover analysis*

16

432   In the previous section, 100% soy and 100% alfalfa ideal simulations were used to estimate
433   the long-term changes in the water fluxes. However, we would like to estimate the effect of a
434   transient land cover which is similar to what happened historically (Figure 2). To estimate the
435   transient moisture and energy fluxes, we used the yearly land cover changes for the region from
436   Figure 2. It is important to highlight that, in reality, land cover in the region changed from mostly
437   grasses and perennial crops like alfalfa, to a mixture of annual crops including soy, corn, wheat
438   and other crops. Our simulations greatly simplify this complexity by assuming that the land
439   cover is composed of a mixture of only alfalfa and soy. Furthermore, we do not account for the
440   use of cover crops, despite the fact that these are sometimes used during the winter months. This
441   will provide a first-order idea of the transient fluxes but will likely not reflect the actual historical
442   conditions. The annual values were calculated based on a weighted "tile" approach commonly
443   used in land surface models. For example, i^{th} year values of latent heat flux (LH_i) were calculated
444   as

$$ LH_i = \frac{LH_{alfalfa} * (\% \, alfalfa) + \, LH_{soy} * (\% \, soy)}{100} $$

445   This method was followed for other variables as well (Figure 12a-12d). The figures reveal that
446   a gradual land use change pattern from alfalfa to soy, results in decreased LHF and increase
447   SHF. Similarly, annual recharge and runoff increases over time. Our results show a decreasing
448   trend of ET, increasing trend of SHF, increasing trend of annual recharge (not statistically
449   significant), and increasing trend of surface runoff (not statistically significant). Nonetheless,
450   these long-term trends agree in sign with the observations. Increased recharge and runoff are
451   reflected in increased baseflow and storm flow of Carcarañá river (Figure 4). Along with
452   decreasing water table depth, this poses a higher flooding risk in the region in recent years,
453   which is reported in many studies (Aragón et al., 2010, Nosetto et al., 2012).

454   Finally, we argue that the change in water table depth over the years is partially linked to the
455   transient recharge estimates. It is important to highlight that we are not directly simulating
456   absolute values of water table depth because we lack information about the specific yield of the
457   unconfined aquifer and because we cannot simulate lateral groundwater flow in the one-column
458   Noah-MP configuration (Niu et al., 2007). Due to these uncertainties in the groundwater scheme,
459   we can only infer how changes in the water table depth could be related to changes in recharge.
460   We see a slight increase (not statistically significant) in annual recharge throughout the period
461   (Figure 12c), and therefore, the simulated trend in recharge would not solely account for the 10m
462   decrease in water table depth found in observations (Figure 4a). However, we find significant
463   temporal correlation (R = 0.54) between interannual changes in water table depth change and
464   transient recharge (Figure 13). This indicates that changes in recharge driven primarily by
465   climate variability as represented by Noah-MP, correlate well with water table depth
466   observations. This result agrees with Mercau et al. 2015, who related annual changes in water
467   table depth to annual balance between precipitation and evaporation (P-E). However, these
468   changes are also controlled by the type of vegetation. For example, changes in water table depth
469   are more pronounced when there is soy rather than alfalfa (Figure 14). This is notable in the El
470   Niño years (when precipitation is higher than normal in SESA, Cai et al., 2020). While alfalfa

471   can still use most of the excess water as ET, land planted with soy experiences comparatively
472   larger changes in water table depth (with the help of more recharge, from Figure 13). This can
473   pose a difference of as large as 1 m between these two vegetation types. In the La Niña years
474   (precipitation below normal in SESA), vegetation las less impact on water table depth change,
475   since less water is available for recharge. Hence, we conclude that interannual variability in
476   recharge, and groundwater table depth are partially controlled by interannual climate variability
477   and partially controlled by vegetation type. As such, the probability of large changes in water
478   table depth during ENSO events is exacerbated when the land cover is switched from alfalfa to
479   soy.

480

481
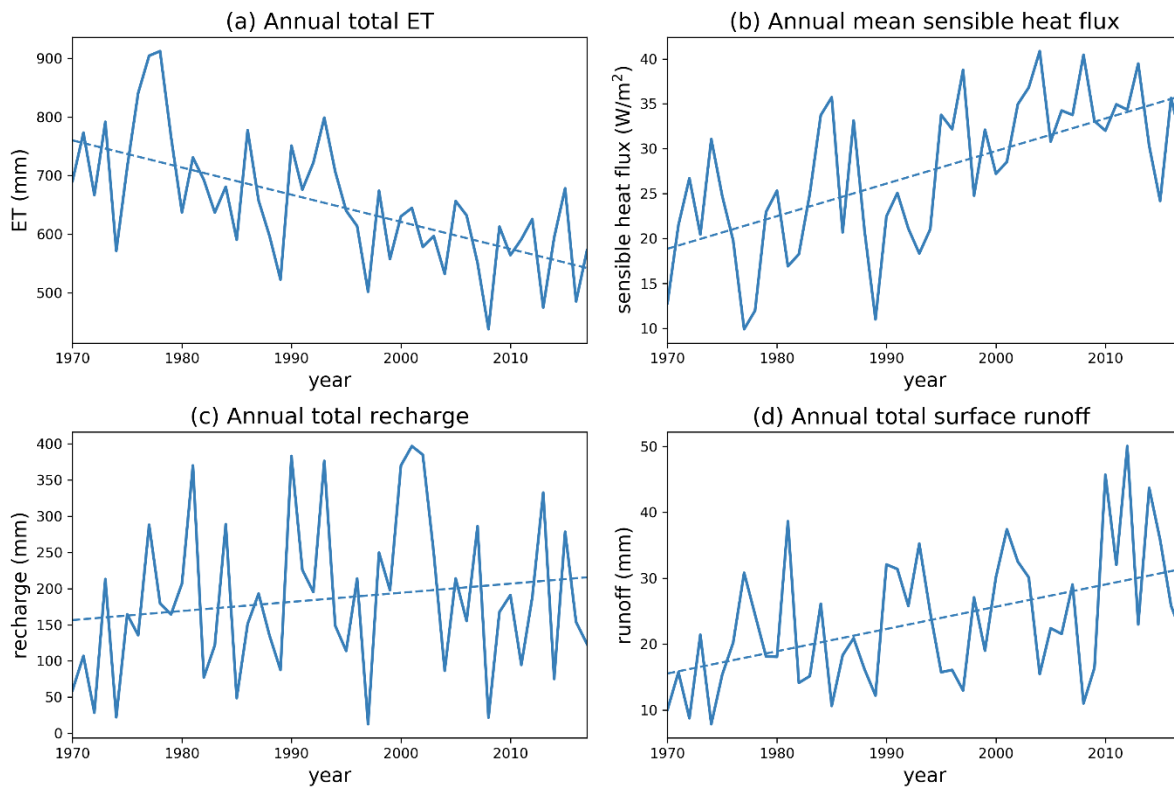
Figure 12. Long term estimates of annual mean (a) latent heat flux, (b) sensible heat flux (c)
recharge (d) runoff and (e) water table depth according to the land use estimates of Figure 2. The
dashed lines show the linear trends. Decreasing trend of ET was found statistically significant at
95% (p = 6.6×10^{-6}), increasing trend of SHF was found statistically significant at 95% (p =
2.07×10^{-5}), increasing trend of annual recharge was not found statistically significant at 95% (p =
0.2665), increasing trend of surface runoff was not found statistically significant at 95% (p =
0.0016).

489   **4. Conclusions**

490   In the past decades, there has been a dramatic shift of land cover in central Argentina from
491   perennial to annual crops. These changes came about due to technological advances, global

492   economic shifts and national policies. In this work we use detailed observations and modeling to
493   understand how the shift in land cover has also affected the sub-surface, surface and atmospheric
494   fluxes of moisture and energy. Long-term observations have shown that, despite slightly
495   decreasing precipitation, streamflow in the region has increased primarily due to baseflow. In
496   addition, water table depth has decreased significantly since the 1970s. The RELAMPAGO field
497   campaign provided us the opportunity to observe the hydrometeorology of the region using a
498   paired eddy-covariance tower site in Marcos Juarez, Argentina. We installed the towers within
499   the INTA experimental station which has an alfalfa experimental site along with soy crops. The
500   alfalfa experimental site reflects conditions similar to those that prevailed in the 1970s, while the
501   soy site is characteristic of the land cover of today.

502   Our observations reveal that ET and specific humidity are higher at the alfalfa site, particularly
503   for the period of July-December. The alfalfa site also has deeper water table depth. On the other
504   hand, sensible heat, outgoing shortwave radiation and soil temperature are higher at the soy site.
505   The higher sensible heat in the soy crop between June and December is particularly striking. No
506   significant differences were found in the other variables such as 2-m temperature, U- and V-
507   momentum and incoming shortwave radiation. These observations were also used to calibrate
508   Noah-MP land surface model parameters for this region.
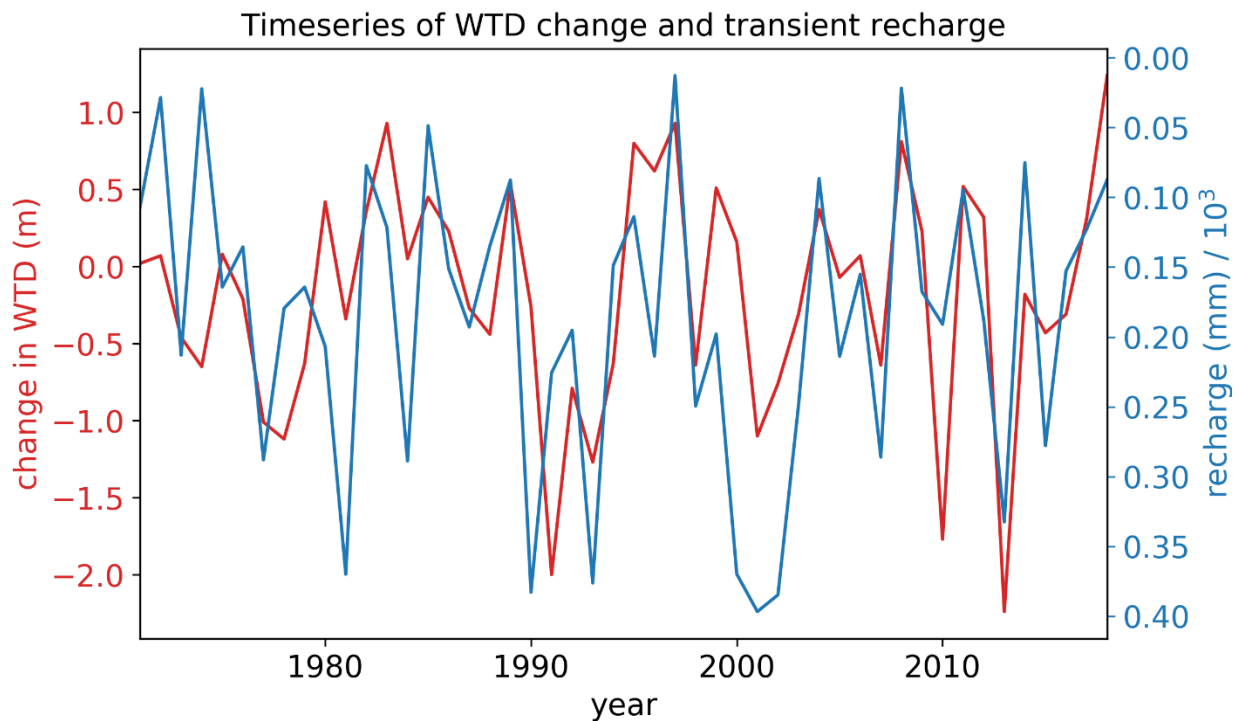
509

510   **Figure 13.** Timeseries of transient Noah-MP recharge and observed inter-annual variation in
511   water table depth.

19

512   Long-term Noah-MP simulations reveal that different land-surface properties affect the
513   partitioning of rainfall between ET, recharge and runoff. ET is significantly higher for alfalfa.
514   Long term simulations reveal that ~95% of precipitation is evaporated in the alfalfa site with


515
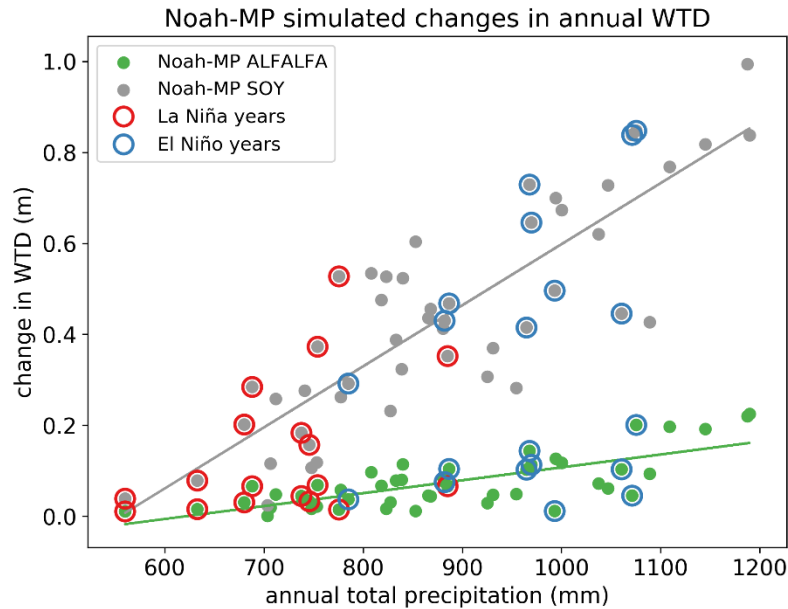
Figure 14. Effect of vegetation on the changes in WTD in different climatic years as simulated
by Noah-MP. El Niño and La Niña years were identified based on Oceanic Niño Index
(https://ggweather.com/enso/oni.htm). The solid lines show the linear trends in the data.

519   negligible recharge and runoff. On the other hand, ET in the soy site accounts for ~68% of
520   precipitation. The recharge significantly increases in case of soy (~28% from ~5% in alfalfa).
521   Runoff also increases from 0.9% in alfalfa to 3.5% in soy. Significantly higher recharge in soy
522   would result in higher baseflow and shallower water table, as we have seen in the observations.
523   However, the simulated increase in recharge in the transient simulation is not able to account for
524   the dramatic observed change in water table depth. It is important to highlight that our
525   experimental setup is highly simplified, with predefined LAI and root values and only one crop
526   type in each simulation. More realistic estimates would require flux tower observations over
527   other types of crops such as winter wheat, corn and cover crops. These land cover types likely
528   have characteristic moisture and energy fluxes in between the soy and alfalfa. Furthermore, we
529   do not explicitly simulate water table depth due to the fact that the one-dimensional model does
530   not account for lateral groundwater flow and unknown aquifer related data. However, these
531   results show that, given identical climate conditions, the different land covers result in a very
532   different partitioning of precipitation. Higher recharge in the soy scenario contributes to higher
533   water table depth and more runoff. The effect on water table depth is even more pronounced in
534   El Niño years when higher than normal precipitation is available, and the soy scenario shows
535   more significant changes in water table depth than the alfalfa scenario.

Our results suggest that the large-scale changes in land cover in Argentina have likely affected sub-surface, surface and atmospheric fluxes of moisture and energy. When compared to perennial land cover, annual crops such as soy result in a shallower and more variable water table, increased runoff driven by baseflow increases, decreased ET and increased sensible heat. In other words, much of the water that was going into the atmosphere in the 1970s is now going into the surface and subsurface. Furthermore, the energy that was being used to evaporate the water is now going into sensible heat, and this results in a dramatic 250% increase in the Bowen ratio. The implications of this shift in atmospheric fluxes of moisture and energy will be the focus of future work.

Acknowledgments, Samples, and Data

References

Aragón, R., E. G. Jobbágy, and E. F. Viglizzo (2010), Surface and groundwater dynamics in the sedimentary plains of the Western Pampas (Argentina), *Ecohydrol.*, 4(3), 433–447, doi:10.1002/eco.149.

Baldi G and Paruelo J M (2008), Land-use and land cover dynamics in South American temperate grasslands Ecol. Soc. 13 6

Ball, J.T., Woodrow, I.E., Berry, J.A., 1987. A Model Predicting Stomatal Conductance and its Contribution to the Control of Photosynthesis under Different Environmental Conditions, in: Progress in Photosynthesis Research. Springer Netherlands, Dordrecht, pp. 221–224. https://doi.org/10.1007/978-94-017-0519-6_48

Cai, W., McPhaden, M.J., Grimm, A.M. *et al.* Climate impacts of the El Niño–Southern Oscillation on South America. *Nat Rev Earth Environ* **1,** 215–231 (2020). https://doi.org/10.1038/s43017-020-0040-3

Cai, X., Z.-L. Yang, C. H. David, G.-Y. Niu, and M. Rodell, 2014: Hydrological evaluation of the Noah-MP land surface model for the Mississippi River Basin. J. Geophys. Res. Atmos., 119, 23–38, https://doi.org/10.1002/2013JD020792.

574 Chen, F., and J. Dudhia (2001), Coupling an advanced land surface-hydrology model with the
575 Penn State-NCAR MM5 modeling system. Part I: Model implementation and sensitivity, Mon.
576 Weather Rev., 129(4), 569–585.

577 Cuntz, M., J. Mai, L. Samaniego, M. Clark, V. Wulfmeyer, O. Branch, S. Attinger, and S.
578 Thober (2016),The impact of standard andhard-coded parameters on the hydrologic fluxes in the
579 Noah-MPland surface model, J. Geophys.Res. Atmos., 121, 10,676–
580 10,700,doi:10.1002/2016JD025097.

581 Duan, Q., V. K. Gupta, and S. Sorooshian (1993), Shuffled complex evolution approach for
582 effective and efficient global minimization, J. Optim. Theory Appl., 76(3), 501–521.

583 Eckhardt, K., 2012. Technical note: analytical sensitivity analysis of a two parameter recursive
584 digital baseflow separation filter. Hydrol. Earth Syst. Sci. 16,451–455.

585 Farquhar, G.D., von Caemmerer, S., Berry, J.A., 1980. A biochemical model of photosynthetic
586 CO2 assimilation in leaves of C3 species. Planta 149, 78–90.
587 https://doi.org/10.1007/BF00386231

588 García, A. G., Di Bella, C. M., Houspanossian, J., Magliano, P. N, Jobbágy, E. G., Posse, G., …
589 Nosetto, M. D. (2017a). Patterns and controls of carbon dioxide and water vapor fluxes in a dry
590 forest of Central Argentina. Agricultural and Forest Meteorology, 247,520–532.

591 García Pablo E., Angel N. Menénendez, Guillermo Podestá, Federico Bert, Poonam Arora &
592 Esteban Jobbágy (2017b) Land use as possible strategy for managing water table depth in flat
593 basins with shallow groundwater, International Journal of River Basin Management, 16:1, 79-
594 92, DOI: 10.1080/15715124.2017.1378223

595 Gochis, D.J., M. Barlage, A. Dugger, K. FitzGerald, L. Karsten, M. McAllister, J. McCreight, J.
596 Mills, A. RafieeiNasab, L. Read, K. Sampson, D. Yates, W. Yu, (2018). The WRF-Hydro
597 modeling system technical description, (Version 5.0). NCAR Technical Note. 107 pages.
598 https://ral.ucar.edu/sites/default/files/public/WRF-HydroV5TechnicalDescription.pdf, Source
599 Code DOI:10.5065/D6J38RBJ

600 Giménez, R, Mercau, JL, Bert, FE, et al. Hydrological and productive impacts of recent land-use
601 and land-cover changes in the semiarid Chaco: Understanding novel water excess in water scarce
602 farmlands. Ecohydrology. 2020; e2243. https://doi.org/10.1002/eco.2243

603 Graesser, J., T. M. Aide, H. R. Grau, and N. Ramankutty (2015), Cropland/pastureland dynamics
604 and the slowdown of deforestation in Latin America, Environ. Res. Lett., 10(3), 034017–11,
605 doi:10.1088/1748-9326/10/3/034017.

606 Houska, T., Kraft, P., Chamorro-Chavez, A. and Breuer, L.: SPOTting Model Parameters Using
607 a Ready-Made Python Package, PLoS ONE, 10(12), e0145180,
608 doi:10.1371/journal.pone.0145180, 2015.

Jobbagy Gampel, E. G., M. D. Nosetto, C. S. ssantoni, and G. Baldi (2008), El desafío ecohidrológico de las transiciones entre sistemas leñosos y herbáceos en la llanura Chaco-Pampeana, *Ecologia Austral*, 18, 305–322.

Jobbágy Esteban, Santiago Lorenzo, Ricardo Páez, et al. Plants vs. Streams: Their groundwater-mediated competition at "El Morro", a developing catchment in the dry plains of Argentina. *Authorea.* September 28, 2020. **DOI:** 10.22541/au.160133536.67833093

Kuppel, S., J. Houspanossian, M. D. Nosetto, and E. G. Jobbágy (2015), What does it take to flood the Pampas?: Lessons from a decade of strong hydrological fluctuations, *Water Resour Res*, 51(4), 2937–2950, doi:10.1002/2015WR016966.

Mercau Jorge L., Marcelo D. Nosetto, Federico Bert, Raúl Giménez, Esteban G. Jobbágy, Shallow groundwater dynamics in the Pampas: Climate, landscape and crop choice effects, Agricultural Water Management, Volume 163, 2016, Pages 159-168, ISSN 0378-3774, https://doi.org/10.1016/j.agwat.2015.09.013.

Lee, E., Livino, A., Han, SC. *et al.* Land cover change explains the increasing discharge of the Paraná River. *Reg Environ Change* **18,** 1871–1881 (2018). https://doi.org/10.1007/s10113-018-1321-y

Martinez, J. A., Dominguez, F., & Miguez-Macho, G. (2016a). Effects of a groundwater scheme on the simulation of soil moisture andevapotranspiration over southern South America.Journal of Hydrometeorology, 17, 2941–2957.https://doi.org/10.1175/JHM-D-16-0051.1

Martinez, J.A., F. Dominguez, and G. Miguezmacho. 2016b. Impacts of a groundwater scheme on hydroclimatological conditions over southern South America. J. Hydrometeorol. 17:2959–2978.https://doi.org/10.1175/JHM-D-16-0052.1

Miguez-Macho, G., and Y. Fan, 2012: The role of groundwater in the Amazon water cycle: 1. Influence on seasonal streamflow, flooding and wetlands. J. Geophys. Res., 117, D15113, doi:10.1029/2012JD017539.

Modarres, R., Sarhadi, A., 2009. Rainfall trends analysis of Iran in the last half of the twentieth century. J. Geophys. Res. 114.

National Secretary of Water Resources https://www.argentina.gob.ar/obras-publicas/hidricas/base-de-datos-hidrologica-integrada

Nesbitt, S. W., and Coauthors, 2016: RELAMPAGO Experimental Design Overview. Accessed 15 April 2020, https://www.eol.ucar.edu/field_projects/relampago.

Niu, G.-Y., Z.-L. Yang, R. E. Dickinson, L. E. Gulden, and H. Su (2007), Development of a simple groundwater model for use in climate modelsand evaluation with Gravity Recovery and Climate Experiment data,J. Geophys. Res., 112, D07103, doi:10.1029/2006JD007522.

Niu, G.-Y., et al. (2011), The Community Noah Land Surface Model withMulti-Parameterization Options (NOAH-MP): 1. Model description and evaluation with local-scale measurements, J. Geophys. Res., 116,D12109, doi:10.1029/2010JD015139.

646 Nosetto M.D., E.G. Jobbágy, A.B. Brizuela, R.B. Jackson, The hydrologic consequences of land
647 cover change in central Argentina Agric. Ecosyst. Environ., 154 (2012), pp. 2-11

648 Nosetto, M. D., R. A. Paez, S. I. Ballesteros, and E. G. Jobbágy (2015), Higher water-table levels
649 and flooding risk under grain vs. livestock production systems in the subhumid plains of the
650 Pampas, *Agriculture, Ecosystems and Environment*, 206, 60–70, doi:10.1016/j.agee.2015.03.009.

651 Nosetto MD, Luna Toledo E,Magliano PN, Figuerola P, Blanco LJ, Jobbágy EG. Contrasting
652 CO2 and water vapour fluxes in dry forest and pasture sites of central Argentina. Ecohydrology.
653 2020; e2244. https://doi.org/10.1002/eco.2244

654 Pal, S., H.-I. Chang, C. L. Castro, and F. Dominguez, 2019: Credibility of convection-permitting
655 modeling to improve seasonal precipitation forecasting in the southwestern United States. Front
656 Earth Sci., 7, 11, https://doi.org/10.3389/feart.2019.00011.

657 Pal, S., Dominguez, F., Dillon, M. E., Alvarez, J., Garcia, C. M., Nesbitt, S. W., & Gochis, D.
658 (2021). Hydrometeorological Observations and Modeling of an Extreme Rainfall Event Using
659 WRF and WRF-Hydro during the RELAMPAGO Field Campaign in Argentina, Journal of
660 Hydrometeorology, 22(2), 331-351. doi: https://doi.org/10.1175/JHM-D-20-0133.1

661 Paruelo, J. M., J. P. guerschman, and S. R. Veron (2005), Expansion Agricola y cambios en el
662 uso del suelo, Ciencia Hoy, 1–10.

663 Rodell, M., and Coauthors, 2004: The Global Land Data Assimilation System. Bull. Amer.
664 Meteor. Soc., 85, 381–394, doi:10.1175/BAMS-85-3-381.

665 Rodriguez P., Raúl Giménez, Marcelo D. Nosetto, Esteban G. Jobbágy, Patricio N. Magliano,
666 Changes in water fluxes partition related to the replacement of native dry forests by crops in the
667 Dry Chaco, Journal of Arid Environments, Volume 183, 2020, 104281, ISSN 0140-1963,
668 https://doi.org/10.1016/j.jaridenv.2020.104281.

669 Ruscica, R. C., Sörensson, A. A., & Meńendez, C. G. (2015). Pathways between soil moisture
670 and precipitation in southeastern South America.Atmospheric Science Letters, 16(3), 267–272.

671 Sellers, P. J., et al. (1997), Modeling the exchanges of energy, water, and carbon between
672 continents and the atmosphere, Science, 275 (5299),502–509.

673 Schilling, K. E., K.-S. Chan, H. Liu, and Y.-K. Zhang (2010), Quantifying the effect of land use
674 land cover change on increasing discharge in the Upper Mississippi River, *Journal of Hydrology*,
675 387(3-4), 343–345, doi:10.1016/j.jhydrol.2010.04.019.

676 Schilling, K. E., M. K. Jha, Y.-K. Zhang, P. W. Gassman, and C. F. Wolter (2008), Impact of
677 land use and land cover change on the water balance of a large agricultural watershed: Historical
678 effects and future directions, *Water Resour Res*, 44(7), 563–12, doi:10.1029/2007WR006644.

679 Shuttleworth WJ. Evaporation. In: Maidment DR, ed. Handbook of Hydrology. New York:
680 McGraw-Hill, Inc.; 1993, 4.1–4.53.

681 Sneyers, R., 1990. On statistical analysis of series of observation. Technical note No.143, WMO
682 No. 415. World Meteorological Organization, Geneva.

683 Viglizzo, E. F., E. G. Jobbágy, L. Carreño, F. C. Frank, R. Aragón, L. D. Oro, and V. Salvador
684 (2009), The dynamics of cultivation and floods in arable lands of Central Argentina, *Hydrol*
685 *Earth Syst Sc*, 13(4), 491–502, doi:10.5194/hess-13-491-2009.

686 Xu, X., B. R. Scanlon, K. Schilling, and A. Sun (2013), Relative importance of climate and land
687 surface changes on hydrologic changes in the US Midwest since the 1930s: Implications for
688 biofuel production, *Journal of Hydrology*, 497(C), 110–120, doi:10.1016/j.jhydrol.2013.05.041.

689 Yaeger, M. A., M. Sivapalan, G. F. McIsaac, and X. Cai (2013), Comparative analysis of
690 hydrologic signatures in two agricultural watersheds in east-central Illinois: legacies of the past
691 to inform the future, *Hydrol. Earth Syst. Sci.*, 17(11), 4607–4623, doi:10.5194/hess-17-4607-
692 2013.

693 Zellner Moira, Guillermo A. García, Federico Bert, Dean Massey, Marcelo Nosetto, Exploring
694 reciprocal interactions between groundwater and land cover decisions in flat agricultural areas
695 and variable climate, Environmental Modelling & Software, Volume 126, 2020, 104641, ISSN
696 1364-8152, https://doi.org/10.1016/j.envsoft.2020.104641.

697 Zeng, J., Zhang, Q. The trends in land surface heat fluxes over global monsoon domains and
698 their responses to monsoon and precipitation. *Sci Rep* **10,** 5762 (2020).
699 https://doi.org/10.1038/s41598-020-62467-0

700 Zhang, Y. K., and K. E. Schilling (2006), Increasing streamflow and baseflow in Mississippi
701 River since the 1940s: Effect of land use change, *Journal of Hydrology*, 324(1-4), 412–422,
702 doi:10.1016/j.jhydrol.2005.09.033.

703 Zheng, H., Yang, Z. L., Lin, P. R., Wei, J. F., Wu, W. Y., Li, L. C., et al. (2019). On the
704 sensitivity of the precipitation partitioning into evapotranspiration and runoff in land surface
705 parameterizations. Water Resources Research, 55,95–111.
706 https://doi.org/10.1029/2017WR022236

707

708

709